IEEE Photonics Journal
An IEEE Photonics Society Publication

The Correction of Nonlinearity in Wavelength Scanning Based on Long-OPD Interferometer for Fiber Bragg Grating Demodulation in Environment With Variable Temperature

Volume 12, Number 2, April 2020

Xuezhi Zhang
Yue Chu
Junfeng Jiang
Kun Liu
Xiaojun Fan
Bangtian Xu
Lei Jiang
Yuqing Li
Tiegen Liu

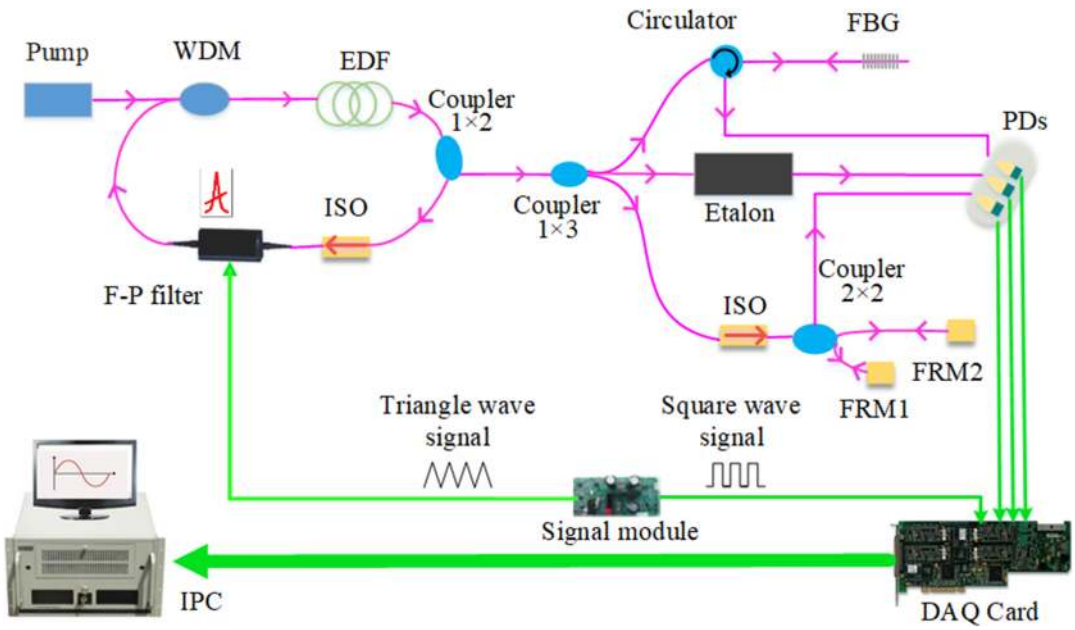

DOI: 10.1109/JPHOT.2019.2963237

The Correction of Nonlinearity in Wavelength Scanning Based on Long-OPD Interferometer for Fiber Bragg Grating Demodulation in Environment With Variable Temperature

Xuezhi Zhang,[1,2,3] **Yue Chu**,[1,2,3] **Junfeng Jiang**,[1,2,3] **Kun Liu**,[1,2,3] **Xiaojun Fan**,[1,2,3] **Bangtian Xu**,[1,2,3] **Lei Jiang**,[1,2,3] **Yuqing Li**,[1,2,3] **and Tiegen Liu** [1,2,3]

[1]School of Precision Instrument and Opto-electronics Engineering, Tianjin University, Tianjin 300072, China
[2]Key Laboratory of Opto-electronics Information Technology, Ministry of Education, Tianjin 300072, China
[3]Tianjin Optical Fiber Sensing Engineering Center, Institute of Optical Fiber Sensing of Tianjin University, Tianjin 300072, China

DOI:10.1109/JPHOT.2019.2963237

Manuscript received October 22, 2019; accepted December 25, 2019. Date of publication December 30, 2019; date of current version March 9, 2020. This work was supported in part by the National Key Research and Development Plan of China under Grant 2016YFC0401902 and in part by the National Natural Science Foundation of China under Grants U1833104, 61735011, 61675152, and 61405139.
Corresponding author: Junfeng Jiang (e-mail: jiangjfjxu@tju.edu.cn).

Abstract: Fabry-Perot (F-P) filter based fiber Bragg grating (FBG) demodulation has been widely applied in many areas. However, the F-P filter suffers from random fluctuation in wavelength scanning when the ambient temperature changes severely, which reduces the demodulation accuracy inevitably. In this paper, a demodulation method based on an etalon and a fiber-optic Michelson interferometer is proposed to improve the demodulation accuracy in an environment with variable temperature. The experiment is carried out by constructing an interferometer with long-optical path difference (OPD). When the environment temperature increases from 20 °C to 60 °C in 30 minutes, the results show that the error of the proposed method is reduced from ± 20.39 pm to ± 6.89 pm. The standard deviation is 3.11 pm, which is reduced by 43.92% compared with the etalon-based demodulation method.

Index Terms: Michelson interferometer, optical fiber sensor, filter nonlinearity, variable temperature environment demodulation.

1. Introduction

Fiber Bragg Grating (FBG) has been widely applied to aerospace, nuclear industry, civil engineering, petrochemical and some other fields because of its advantages in harsh environment, such as small size, lightweight, immune to electromagnetic interference, and so on [1], [2]. The FBG demodulation method based on tunable Fabry-Perot (F-P) filter is a reliable demodulation method with high accuracy, which has been widely employed in various fields [3], [4]. The F-P filter is driven by a triangle signal according to the inverse piezoelectric effect, and generates output

light with scanning wavelength [5]–[7]. However, the operating environment will suffer from severe temperature variation in some application areas, such as highland, desert or space. In this situation, the piezoelectric ceramic transducer (PZT) in F-P filter may exhibit hysteresis, creep and nonlinear dynamic effects [8]. These effects will cause the non-repeatable wavelength scanning, affecting the accuracy and stability of demodulation. A TEC cooler can control environment temperature changes, however, it takes several seconds for TEC to work in the environment of variable temperature, during which PZT will still perform nonlinear effect. Besides, the large size and heavy weight of the TEC may increase the complexity of the system structure, and much more power consumption is required. So the TEC is not suitable for the application of some areas, for example in aerospace.

In order to solve this problem, some wavelength reference methods have been proposed, such as FBGs reference [9], [10], acetylene gas absorption spectrum reference [11] and F-P etalon [12]. Among these methods, multiple FBGs with different central wavelengths are employed in the method based on reference of FBGs to describe the nonlinear effect of F-P filter. However, it is difficult to ensure temperature characteristic of sensing FBGs and reference FBGs are identical [9], [10]. The method based on acetylene gas absorption spectrum reference performs better in correcting the nonlinear movement of PZT, especially in variable temperature environment. But the wavelength range of demodulation is limited by the wavelength distribution of absorption peaks [11]. The method based on F-P etalon can provide multiple peaks with equal spacing in the frequency domain for reference. This method has significant advantages in accuracy by suppressing the ambient temperature fluctuation [12]. However, the FSR of the commercial etalon is 25 GHz$\sim$100 GHz, which limits the effect of the nonlinearity correction for FBG demodulation in a variable temperature environment.

In this paper, a demodulation method based on F-P etalon and Michelson interferometer with a long optical path difference (OPD) is proposed, which can correct the nonlinearity and improve the PZT performance in F-P filter. Optical interferometry has the advantages of high sensitivity, high stability, and relatively cost-effective, which has been widely studied and applied in many areas [13]–[18]. Selwan K *et al.* [15] designed a Mach–Zehnder interferometer with the FSR of 16pm in their optical interrogator for high precision measurement. A series of reference frequency is supplied in demodulation by the interferometry, which is equivalent to employ an etalon with ultra-narrow FSR. The OPD is designed as long as it is possible to reduce the interference fringe spacing. The reference wavelength between the adjacent peaks of the etalon is divided into fine grid by the interference fringe. The Bragg wavelength of the FBG is determined by the F-P etalon and the interferometer together. This method restrains the impact of temperature fluctuation by compensating the nonlinearity between the drive voltage and the movement of PZT. Experimental results show that the demodulation accuracy is improved from $\pm$ 20.39 pm to $\pm$ 6.89 pm when the demodulation system is placed in a temperature-changing environment.

2. Principle

2.1 System Principle

In the F-P etalon based demodulation method [12], if there is a perfect linear relationship between the voltage applied on the PZT and the output wavelength of the F-P filter, the sampling points between the adjacent peaks of the etalon will be the same when a triangular wave is imposed on the filter. The Bragg wavelength of the FBG can be obtained exactly by interpolation. However, the relationship between the voltage applied on the PZT, and the transmittance wavelength of the F-P filter is impacted by the ambient temperature seriously. The nonlinearity of the inverse piezoelectric effect in PZT results in different wavelength scanning speed of filter at different wavebands, which will affect the demodulation accuracy. This effect must be considered if the demodulation system is operated in the environment with severe temperature change.

FBG sensing demodulation system based on Michelson interferometer with long OPD is proposed to solve this problem, which is shown in Fig. 1. The scanning light source module consists of

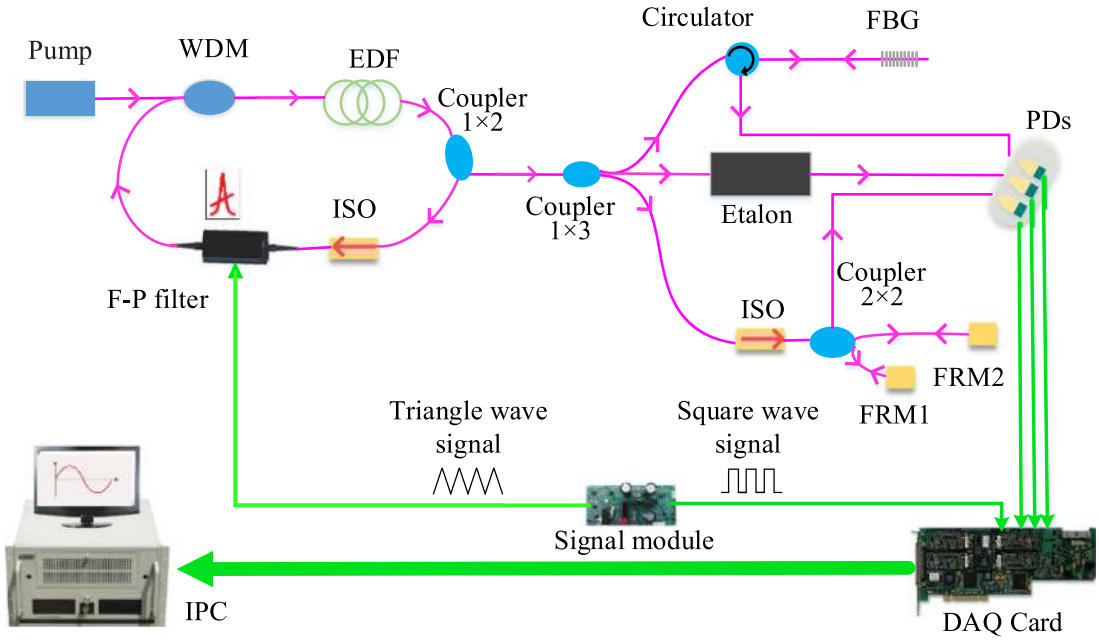

Fig. 1. Schematic diagram of FBG sensing demodulation system based on long-OPD Michelson interferometer.

a laser diode (Pump), wavelength division multiplexer (WDM), Erbium-doped fiber (EDF), isolator (ISO), and F-P filter. A triangle wave is imposed on the F-P filter to generate output light with scanning wavelength. The output light is split into three parts by a 1 × 3 coupler. The first part is sent to the FBG sensor and received by a photodetector (PD). The second part and the third part are detected by PDs after passing through the etalon and Michelson interferometer respectively.

The peaks generated by mult-beam interference in etalon provide a series of reference wavelengths. The Michelson interferometer consists of an ISO, a 2 × 2 coupler and two Faraday rotator mirrors (FRM) with different lengths of fiber optic pigtails. Interference fringes are inserted to subdivide the waveband between adjacent peaks of the F-P etalon. The Bragg wavelength of the FBG is determined by the F-P etalon and the interferometer together. The signals detected by PDs are sent to the industrial personal computer (IPC) by data acquisition (DAQ) card for further processing. The DAQ is controlled by a square wave from a signal generator. The square wave signal and triangle wave signal have the same frequency to ensure the synchronization of data acquisition. The rising edge of the square wave signal is used as a trigger signal of the acquisition, through which the complete spectra of FBG sensor, optical interferometer and the etalon can be collected.

The light source in the F-P filter based FBG demodulation system is usually amplified spontaneous emission (ASE) source [12]. However, the wide output spectrum of ASE light source results in a short coherence length. The interference fringe can be generated if the OPD between the two beams is smaller than the coherence length of the light source. So the coherence length of ASE limits the reduction of interference fringe spacing to great extent. In order to extend the coherence length, a light source module with F-P filter in the resonant cavity is constructed to generate laser with tunable wavelength. In this source module, the pump laser with 980 nm wavelength is emitted by the pump. The pump laser is injected into the EDF through a 980/1550 WDM. A broadband stimulated radiation is generated in the EDF. A F-P filter modulated by external voltage is included in the resonant cavity of light source to select the output wavelength from the broadband stimulated radiation. The reflected light is restrained by an ISO. Then 20% of the power is sent out, while the other 80% power remains in the cavity through a 1 × 2 coupler. Compared

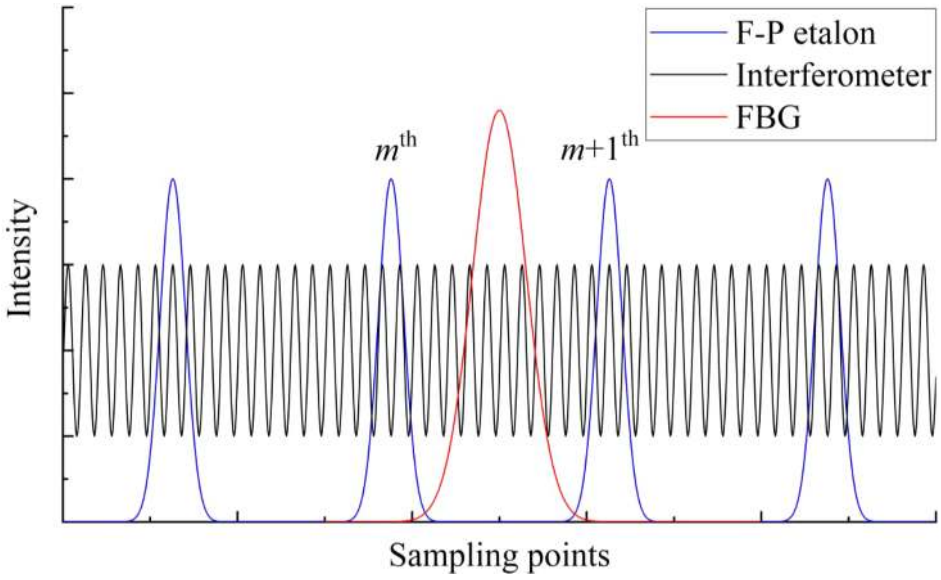

Fig. 2. Position relationship of F-P etalon, interferometer and FBG.

with ASE, the linewidth of this light source is reduced, and the coherence length is increased greatly, which satisfy the requirement of interferometer with long OPD.

2.2 Demodulation Principle

In the demodulation process, triggered by the rising edge of the square wave, the spectra are selected corresponding to the rising edge of triangular wave signal. The reflection peak of FBG, the spectra of the etalon and the interference fringe are shown in Fig. 2 by the red, blue, and black curves, respectively. The Bragg wavelength of FBG is located between the m^{th} and $m+1^{th}$ peak on the etalon spectrum. The interference fringes are inserted between each adjacent peaks of the F-P etalon. The space between the adjacent peaks of the etalon is subdivided by the interference fringes in frequency-domain. The peaks of the etalon spectrum and the interference fringe can act as a role of ruler to measure the Bragg wavelength of the FBG. The interferometer can be considered as a more precise ruler besides the etalon in demodulation, which is the crucial point of this demodulation system to trace the nonlinearity of PZT movement.

The fringe spacing can be expressed as:

$$\Delta f = \left| f_{q+1} - f_q \right| = \frac{c}{2nL} \tag{1}$$

Where f_q and f_{q+1} are the frequency of q^{th} and $q+1^{th}$ order interference fringes, respectively, c represents the speed of light, n denotes fiber refractive index, and L is the geometrical length difference between the two arms of the Michelson interferometer. It is evident that the fringe spacing is inverse proportional to the OPD between two arms of Michelson interferometer. In order to increase the fineness of the ruler, the fringe spacing of the interference should be reduced to be small as possible. As a result, the OPD of this interferometer should be designed to be as long as possible, in order to restrain the demodulation error caused by nonlinear effects of F-P filters in a variable temperature environment.

It is known from the filter principle and experimental results that transmission wavelength decreases with the increase of the drive voltage. The peak positions of etalon spectrum are determined by the centroid algorithm. The specific wavelength value corresponding to each peak of etalon is referred to the calibration file. The etalon transmission peaks on both sides of the

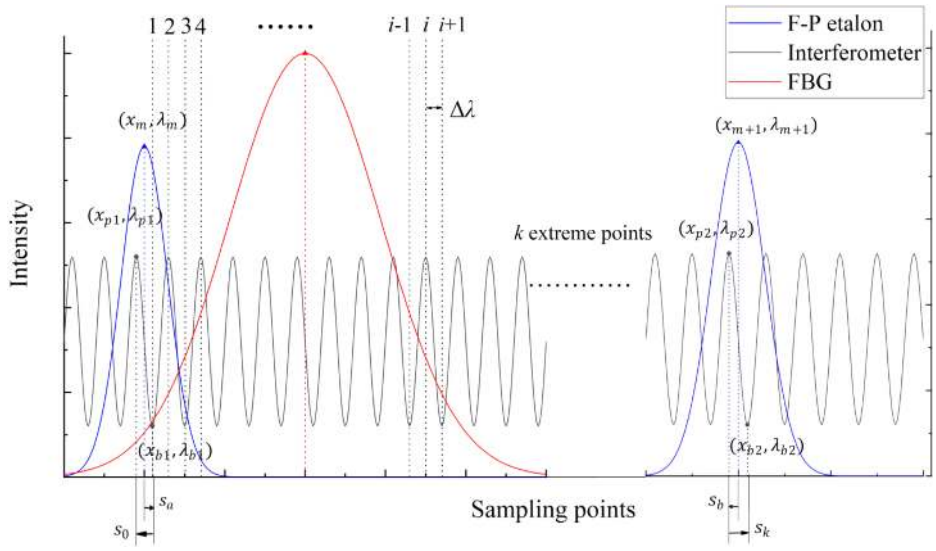

Fig. 3. Demodulation principle of half-width of interference fringes.

FBG reflection peak are marked by m^{th} and $m{+}1^{th}$ peaks. For the interferometer signal, the signal between the m^{th} and $m{+}1^{\text{th}}$ peaks of the etalon which participate in demodulation is selected. The signal is programmed to filter and find the position of the interference fringe's extreme points. In order to improve the accuracy, each extremum point of the interference fringes is used for demodulation, the spacing between adjacent extremum points is half a fringe.

After the extreme position information of the interferometer signal is collected, the demodulation algorithm of the interferometer is expressed in Fig. 3. The number of interference fringes between the m^{th} and $m{+}1^{\text{th}}$ peak of the F-P etalon can be expressed as:

$$\Lambda = \frac{1}{2} \times \left(k - 1 + \frac{s_a}{s_0} + \frac{s_b}{s_k} \right) \tag{2}$$

$$\left(s_a = x_{b1} - x_m, s_0 = x_{b1} - x_{p1}, s_b = x_{m+1} - x_{p2}, s_k = x_{b2} - x_{p2} \right)$$

Where k denotes the number of extreme points between the m^{th} and $m{+}1^{\text{th}}$ peak, s_a represents the number of sampling points between the m^{th} peak of the etalon (x_m) and the first extreme point (x_{b1}) of interferometer behind the m^{th} peak of the etalon (x_m), s_0 represents the number of sampling points between the previous extreme point of interferometer (x_{p1}) and the point (x_{b1}), s_b represents the number of sampling points between the previous extreme point (x_{p2}) of interferometer before the $m{+}1^{\text{th}}$ peak and $m{+}1^{\text{th}}$ peak of the F-P etalon (x_{m+1}), s_k represents the number of sampling points between the point (x_{p2}) and the first extreme point (x_{b2}) of interferometer behind the point (x_{m+1}) as shown in the Fig. 3.

Therefore, the wavelength of extreme points of interference fringes can be described as:

$$\lambda_i = \begin{cases} \lambda_m + \Delta\lambda \times \left| \frac{s_a}{s_0} \right|, & i = 1 \\ \lambda_{i-1} + \Delta\lambda, & 2 \le i \le k \end{cases} \tag{3}$$

$$\Delta\lambda = \frac{\lambda_{m+1} - \lambda_m}{2\Lambda} \tag{4}$$

Where λ_1 denotes the wavelength of the first extreme point of interferometer behind the m^{th} peak of the F-P etalon, λ_i represents wavelength of the i^{th} extreme point, and $\Delta\lambda$ represents the half-width of interference fringe spacing, so $2\Delta\lambda$ represents wavelength of interference fringe spacing.

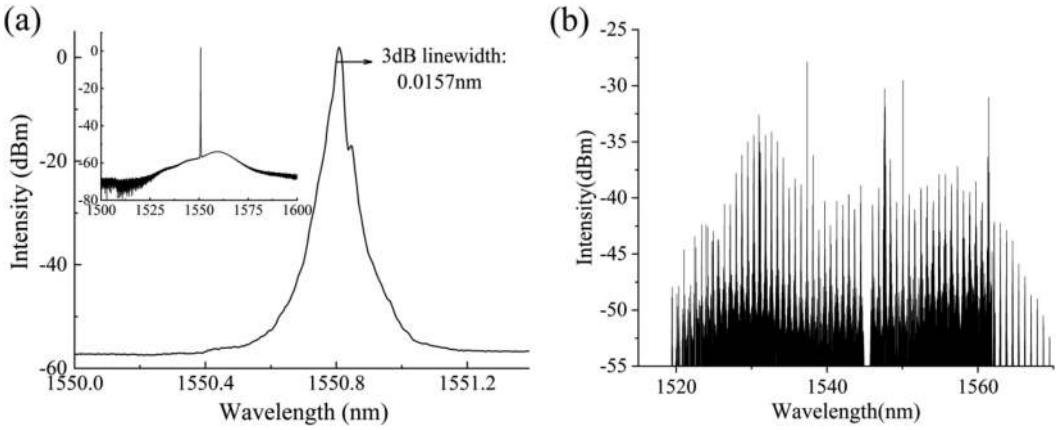

Fig. 4. (a) Spectrum of the output laser by OSA. (b) Spectrum of the etalon by OSA.

The Bragg wavelength of FBG can be calculated by the interpolation between the wavelengths of the two extreme points on interference fringes adjacent to the FBG Bragg wavelength.

When the environment temperature is changed, the OPD between the two arms can be affected due to the thermo-optic effect and thermal expansion effect of the fiber. The relationship between the OPD change and the temperature change ΔT can be expressed as:

$$\Delta OPD = 2n\left(\alpha + \frac{\zeta}{n}\right) L\Delta T \tag{5}$$

Where n represents fiber refractive index, α is the fiber thermal expansion coefficient, ζ is the fiber thermo-optic coefficient, and L is the geometrical length difference between the two arms of the Michelson interferometer. The typical values of n, α, ζ are 1.4682, 5.5 $\times$ 10^{-7}°C-1, and 0.68 $\times$ 10^{-5} °C^{-1}, respectively. For example, when the temperature environment varies between 20 °C and 60 °C, the additional OPD of the interferometer is 15.21 μm if L is 25 mm. Therefore the wavelength variation of fringe spacing induced by environment change can be neglected according to equation (1), and the quantity of interference fringes inserted between the two adjacent peaks of the etalon remains a constant. In other words, the variation of sampling points in fringe spacing distribution is only related to the nonlinearity of PZT, which can guarantee the feasibility of correcting the effect of temperature change.

3. Experiment

For illustrating the advantages of the interferometer based FBG demodulation in a varying temperature environment, the system shown in Fig. 1 is built up in the experiment. In the light source module, the power of pump is 250 mW. The length of the EDF is 2 m. The free spectral range (FSR) of F-P filter (Micron Optics) is 108 nm. Through the 1 $\times$ 2 coupler, 20% of the power in the ring cavity is sent out, while the other 80% of power remains in the cavity. The output power of the light source module is 4.5 mW. The output spectrum is shown in Fig. 4(a). The linewidth of 0.0157 nm of the output light is measured using the optical spectrum analyzer (YOKOGAWA-AQ6370) with a resolution of 0.020 nm. The spectrum of F-P etalon scanned by this laser source module shown in Figure 4(b), reflects the relationship between the output power and the output wavelength of the light source in the C-band.

The tunable F-P filter is driven by a 200 Hz triangle wave. The FSR of the F-P etalon (Prinanex) is 100.02 GHz, the thermal stability of F-P etalon's peak positions is less than 5 pm when the temperature is between -5 °C and 70 °C. The geometrical length difference between the two arms of the Michelson interferometer is 25 mm. The space between adjacent extremum

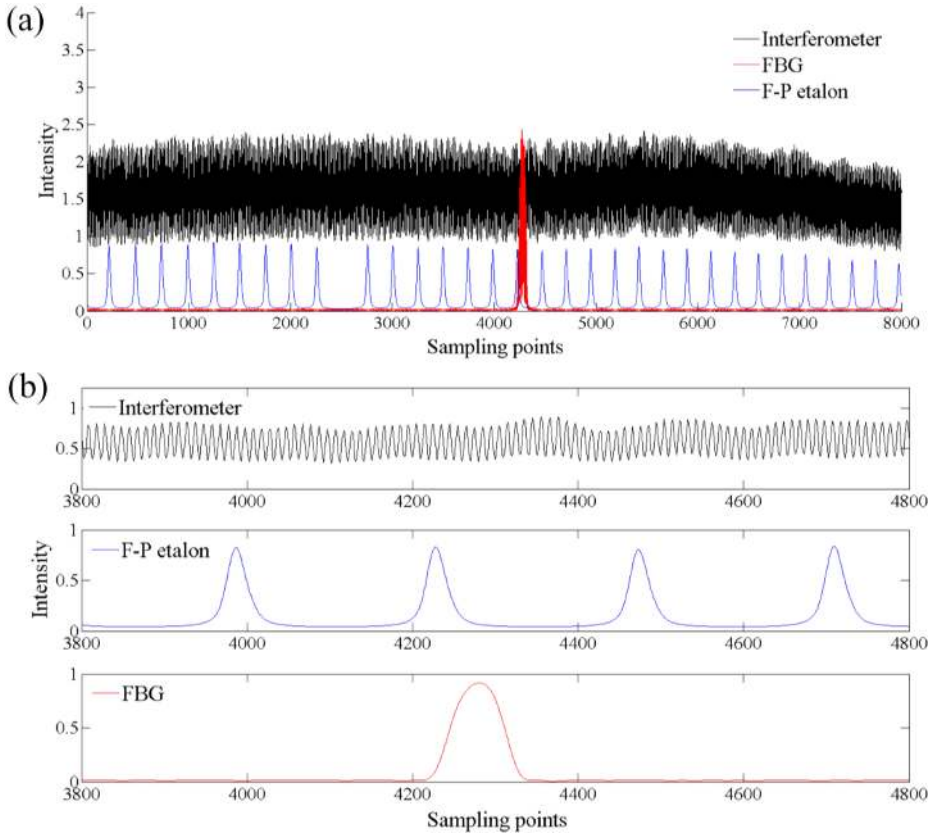

Fig. 5. (a) Original signals detected by PDs. (b) Filtered and normalized signal of each channel around FBG.

points is about 16.5 pm, and the interference fringe spacing in the spectrum generated by this interferometer is about 33 pm correspondingly, so it can provide 24 fringes between adjacent peaks of the etalon. The data sampling rate of the DAQ (NI6115) is 10 MHz for each channel. The temperature sensitivity of the FBG-based sensor is 10.2 pm/°C. The sensing wavelength error caused by temperature fluctuation of the calibrator is ± 0.05 pm. During the experiment, the FBG (MOI) with Bragg wavelengths of 1544.35 nm is placed in metrology well calibrator (Fluke 9170) where the temperature is set to be 25 °C. The temperature stability of the calibrator is as high as ±0.005 °C. The F-P filter, the fiber-optic Michelson interferometer, and the F-P etalon is put into the constant temperature drying oven (Espec), which can provide a varying temperature environments.

A frame of original signal detected during the scanning process is shown in Fig. 5(a). At this time, the environment temperature is 28 °C. The black curve, the red curve and the blue curve represent the signal of interferometer, FBG and etalon, respectively. To illustrate the complicated relationship between these three curves, the normalized signals around the Bragg wavelength of FBG is zoomed in and shown in Fig. 5(b). The random noise is flitted in this figure to make the curves smooth.

The peaks of the etalon and the extreme points of interference signal are both the reference wavelengths in Bragg wavelength determination. The wavelengths of etalon peaks can be known by referring to the calibration file of F-P etalon. The wavelength corresponds to each extreme of interference fringe is determined by equation (2–4), which can be considered as a bridge to connect the peak wavelengths of the etalon and the Bragg wavelength of FBG. The nonlinearity of F-P filter in wavelength scanning described by the F-P etalon and the interferometer is shown in

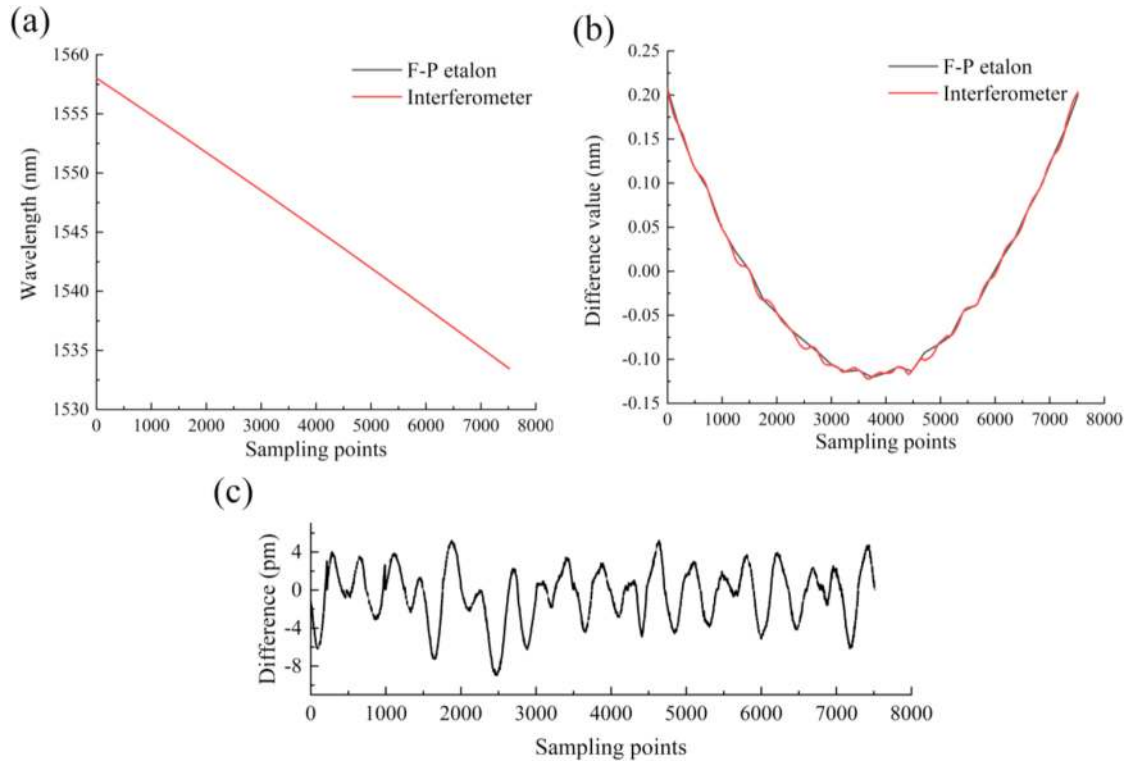

Fig. 6. (a) Wavelength reference - sampling point calibration curve comparison. (b) Subtraction results by fitted line. (c) Difference between two curves.

Fig. 6. Figure 6(a) is the relationship between the sampling point and the transmittance wavelength of F-P etalon. The black curve in this figure is the relationship obtained by etalon, while the result obtained by interference fringes is shown by the red curve. Since the difference between these two curves is only tens of pico-meters, the red curve and the black curve are almost overlapped with each other. In order to see the difference more clearly, a straight line is generated by least-squares fitting based on the data points obtained by etalon only. The fitted line is subtracted from the black curve and red curve in Fig. 6(a) respectively. The subtracted results are shown in Fig. 6(b). Fig. 6(c) shows the difference between the black and red curve in Fig. 6(a). It is evident that the interferometry can provide more detailed points to trace the nonlinearity of filter in wavelength scanning. The interference signal is filtered and the extremum position is found by the centroid method, it's calculated that more than 48 extreme points are inserted between m^{th} and $m+1^{th}$ etalon peaks, which may give great help in correcting the nonlinearity of wavelength scanning induced by PZT.

In order to verify the efficiency of the interference-based demodulation method, the temperature of the oven was set to increase from 20 °C to 60 °C. The FBG is still placed in metrology well calibrator where the temperature is kept to be 25 °C. The experiment lasts 30 minutes. The temperature increasing process is shown in Fig. 7(a). Demodulation result based on etalon only is also calculated for comparison. The Bragg wavelength demodulation results in this process are shown in Fig. 7(b). The black curve and red curve represent the demodulation results based on etalon and interferometer respectively. The initial temperature of the oven is 20 °C, which lasts three minutes. The demodulation results based on the two methods are both relatively stable. From third to eighth minutes, the temperature changes drastically from 24 °C to 56 °C, which corresponds to 10% and 90% in the process of temperature increase. In this stage, as shown by the black curve in Fig. 7(b), the results, demodulated by etalon, begin to oscillate with a

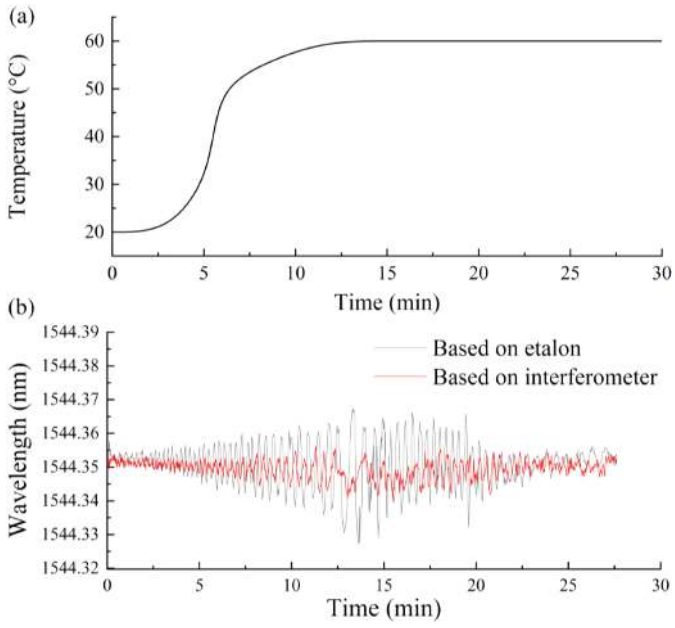

Fig. 7. (a) Temperature change of the oven. (b) Demodulation results based on F-P etalon and interferometer.

maximum amplitude range of 40 pm. The oscillation of demodulation result exhibits hysteresis. In other words, demodulation results will remain oscillate for a while, even though the temperature of the oven has achieved a stable value. Until temperature remains a constant for 20 minutes, the demodulation results return to a stable state. Obviously, the interferometer can effectively suppress the fluctuation of demodulation result compared with the etalon-based method. The error of the etalon based method is as high as $\pm$ 20.39 pm, and the standard deviation is 7.08 pm; while the error of the interferometer based method is reduced to $\pm$ 6.89 pm, and the standard deviation is 3.11 pm. These results show that the interferometer can suppress the nonlinear oscillation of the demodulation effectively. The standard deviation is reduced by 43.92%. It can be seen that the method based on the interferometer has high demodulation accuracy in a varying temperature environment.

As mentioned above, the OPD should be designed to be as long as possible to reduce the interference fringe spacing. However, the reduction of the interference fringe spacing is limited by the interferometry visibility, which is determined by the linewidth of scanning source, and data sampling rate. The fringe visibility will decrease when the linewidth of light source increases which corresponds to an increase in its coherence. If linewidth of the light source is constant, the OPD has a maximum value ($OPD_{\max} = \frac{c}{\Delta f}$). But through the formula $K = \frac{I_{\max} - I_{\min}}{I_{\max} + I_{\min}}$ (K represents the fringe visibility, I_{max} and I_{min} represent the maximum and minimum values of light intensity, respectively), it is necessary that in the pursuit of the quantity of interference fringes, the fringe visibility should also be considered. The OPD of this system is 73.41 mm, the fringe visibility of this system is set to be 0.5, which can satisfy the demand of interference fringe detection and acquisition, and improve the system photoelectric efficiency.

4. Conclusions

A FBG Bragg wavelength demodulation method based on etalon and interferometer with long-OPD is proposed in this paper. Additional reference wavelengths are introduced in the demodulation by the interferometer. This method can correct the nonlinearity in wavelength scanning of the F-P filter when the environment temperature varies severely. The demodulation scheme is discussed both

theoretically and experimentally. More than 48 reference wavelengths are added in the waveband between adjacent peaks on the etalon spectrum. The experimental results show that the error of the conventional method which only uses etalon is up to $\pm$ 20.39 pm and the standard deviation is 7.08 pm when the environment temperature increases from 20 °C to 60 °C. However, the error of the proposed method is reduced to $\pm$ 6.89 pm, and the standard deviation is 3.11 pm. The standard deviation is reduced by 43.92%. This result shows that the interferometer based FBG demodulation method can effectively reduce the impact of environmental temperature variation. This demodulation method will have critical applications in numerous areas, such as desert, space.

References

[1] J. Jiang *et al.*, "Development of optical fiber sensing instrument for aviation and aerospace application," *Proc. SPIE - Int. Soc. Opt. Eng.*, vol. 9044, pp. 1–9, 2013.

[2] P. Nannipieri *et al.*, "Application of FBG sensors to temperature measurement on board of the REXUS 22 sounding rocket in the framework of the U-PHOS project," in *Proc. IEEE Int. Workshop Metrology Aerosp.*, IEEE, pp. 462–467, 2017.

[3] H. W. Lee, and M. Song, "FBG interrogation with a scanning Fabry-Perot filter and Gaussian line-fitting algorithm," in *Proc. Lasers Electro-Opt. Soc., 18th Annu. Meeting IEEE*, pp. 963–964, 2005.

[4] S.-Y. Jeong, S.-J. Choi, and J.-K. Pan, "An improved FBG interrogator considering fiber Fabry-Perot tunable filter nonlinearity," *Adv. Photon., OSA Tech. Dig. (Online)*, paper, JTu2A.55. 2018.

[5] W. Sheng, G. D. Peng, Y. Liu, and N. Yang, "An optimized strain demodulation method for PZT driven fiber Fabry–Perot tunable filter," *Opt. Commun.* vol. 349, pp. 31–35, 2015.

[6] H.-J. Park and M. Song, "Linear FBG temperature sensor interrogation with Fabry-Perot ITU multi-wavelength reference," *Sensors*, vol. 8, no. 10, p. 6769, 2018.

[7] Y. Wang, Y. Cui, and B. Yun, "A fiber-Bragg-grating sensor interrogation system using in-fiber Fabry-Perot interferometer," in *Proc. Int. Conf. Opt. Instruments Technol.: Opt. Sensors Appl.*, International Society for Optics and Photonics, vol. 8199, 2011.

[8] M. Morozov, D. Damjanovic, and N. Setter, "The nonlinearity and subswitching hysteresis in hard and soft PZT," *J. Eur. Ceram. Soc.*, vol. 25, no. 12, pp. 2483–2486, 2005.

[9] H. Ding, X. Wu, J. Liang, and X. Li, "Online calibration of PZT driven fiber Fabry–Perot filter nonlinearity using FBG array and PSO algorithm," *Measurement*, vol. 42, no. 7, 2009.

[10] K. Liu *et al.*, "Investigation of PZT driven tunable optical filter nonlinearity using FBG optical fiber sensing system," *Opt. Commun.*, vol. 281, no. 12, pp. 3286–3290, 2008.

[11] X. Fan *et al.*, "Se marked HCN gas based FBG demodulation in thermal cycling process for aerospace environment," *Opt. Express*, vol. 26, no. 18, pp. 22944–22953, 2018.

[12] G. Yang, J. Guo, G. Xu, L. Lv, G. Tu, and L. Xia, "A novel fiber Bragg grating wavelength demodulation system based on FP etalon," *SPIE/COS Photon. Asia* 2014.

[13] C. Wang and J. Yao, "Ultrafast and ultrahigh-resolution interrogation of a fiber Bragg grating sensor based on interferometric temporal spectroscopy," *J. Lightw. Technol.*, vol. 29, no. 19, pp. 2927–2933, Oct. 2011.

[14] Yi. Jiang, "Stabilized 3 $\times$ 3-coupler-based interferometer for the demodulation of fiber Bragg grating sensors," *Opt. Eng.*, vol. 47, no. 1, pp. 015006-1–015006-6, 2008.

[15] S. K. Ibrahim, M. Farnan, and D. M. Karabacak, "SPIE proceedings photonic instrumentation engineering IV - design of a photonic integrated based optical interrogator," 2017, doi: 10110:101100U.

[16] G. Laffont *et al.*, "Wavelength tunable fiber ring laser for high-speed interrogation of fiber Bragg grating sensors," *Proc. SPIE - Int. Soc. Opt. Eng.*, vol. 5855, pp. 342–346, 2005.

[17] K. Liu *et al.*, "Integrated FBG sensors interrogation using active phase demodulation on a silicon photonic platform," *J. Lightw. Technol.*, vol. 35, no. 16, pp. 3374–3379, Aug. 2017.

[18] Y. Marin, T. Nannipieri, F. Di Pasquale, and C. Oton, "Sixth european workshop on optical fibre sensors - integrated FBG sensors interrogator in silicon photonic platform using active interferometer monitoring," *SPIE Proc.*, vol. 9916, pp. 991626-1–3991626-4, 2016.